Theor Chem Acc (2012) 131:1242
DOI 10.1007/s00214-012-1242-7

REGULAR ARTICLE

Si-embedded graphene: an efficient and metal-free catalyst for CO oxidation by N_2O or O_2

Jing-xiang Zhao · Ying Chen · Hong-gang Fu

Received: 25 March 2012 / Accepted: 21 May 2012 / Published online: 2 June 2012

Abstract As is well known, searching for an efficient catalyst for CO oxidation is of great importance in the removal of poisonous CO gas. From the results of density functional theory calculations, we have reported the catalytic oxidation of CO by O_2 or N_2O on Si-embedded graphene. Both Langmuir–Hinshelwood and Eley–Rideal mechanisms of CO oxidation on Si-embedded graphene were comparably studied. The results indicate that CO oxidation by O_2 on Si-embedded can occur via a two-step mechanism: (1) $CO + O_2 \rightarrow OOCO \rightarrow CO_2 + O$, followed by (2) $CO + O \rightarrow CO_2$. The energy barriers for the two steps are 0.48 and 0.57 eV, respectively. For $N_2O + CO \rightarrow N_2 + CO_2$, N_2O firstly interacts with Si-embedded graphene, releasing N_2 and leaving the O-atom to be attacked by the subsequent CO to yield CO_2 to proceed with the catalytic cycle. The present results provide a useful guidance to fabricate ***metal-free*** graphene-based catalysts for CO oxidation with low cost and high activity.

Keywords CO oxidation · Si-embedded graphene · Density functional theory · Metal-free catalyst

1 Introduction

CO oxidation, although seemingly a simple chemical reaction, provides us with a panacea that reveals the richness and beauty of heterogeneous catalysts [1] and plays an important role in solving the growing environmental problems caused by CO emission from automobiles, industrial processes, and so on. Thus, CO oxidation, often quoted as a textbook example of catalytic reaction, is one of the best-known heterogeneous reactions and can be regarded as a benchmark system [1]. Though earlier studies have shown that some noble metals, such as Pd [2–8], Pt [3, 6–13], Rh [3, 6–9, 14–17], and Au [18–22], can effectively catalyze CO oxidation, the high cost and high reaction temperature for efficient operations impose great limitations to the potential applications of these noble metal catalysts as good catalysts for CO oxidation. Therefore, it is understandable that scientists have been continuously endeavoring to seek suitable catalysts with high activity and lower cost to realize the low-temperature oxidation of CO.

Graphene [23], a single hexagonal atomic sheet, has attracted tremendous attention recently due to its exciting properties and wide applications. Thus, it is expected that graphene has become a rapidly rising star on the horizon of materials science and technology [24–35]. Interestingly, the huge surface-to-volume ratio is advantageous for graphene as a support for heterogeneous catalysts. For example, Fu et al. [36] reported experimentally that Pd nanoparticles supported on graphene exhibit high catalytic for formic acid oxidation. Ajayan et al. [37] found that

Electronic supplementary material The online version of this article (doi:10.1007/s00214-012-1242-7) contains supplementary material, which is available to authorized users.

J. Zhao · H. Fu (✉)
Key Laboratory of Functional Inorganic Material Chemistry, Ministry of Education of the People's Republic of China, Heilongjiang University, Harbin 150080, People's Republic of China
e-mail: fuhg@vip.sina.com

J. Zhao
e-mail: xjz_hmily@yahoo.com.cn

J. Zhao · Y. Chen
Key Laboratory for Design and Synthesis of Functionalized Materials and Green Catalysis, School of Chemistry and Chemical Engineering, Harbin Normal University, Harbin 150025, People's Republic of China

graphene-supported Pt_3Co and Pt_3Cr alloy nanoparticles have high catalytic oxygen-reduction activity. Yoo et al. [38] suggested that small Pt clusters supported on graphene sheets exhibit high catalytic activity for CO oxidation. Theoretically, Au-, Fe-, and Cu-embedded graphenes were predicted to be a highly active catalyst for CO oxidation [39–41], which can be attributed to the partially occupied *d* orbital localized in the vicinity of the Fermi level due to the interaction of the Au-, Fe-, and Cu-atom with graphene. These investigations suggest that graphene is an attractive catalyst through its interaction with metal clusters or a single atom.

We note that precious metals or metal oxides are the commonest catalysts in the current established CO oxidation process, which are often energy-consuming and not highly selective, and wasting resources. Metal-free heterogeneous catalyst, especially carbon-based catalyst, is an interesting alternative to some current industrialized chemical processes. This can be expected, because these metal-free catalysts are friendly to environment and exhibit good thermal conductivity, thereby rendering them good candidates for green chemistry with low emission and an efficient use of the chemical feedstock [42]. In this paper, we performed density functional theory (DFT) calculations to explore the possibility of ***metal-free*** Si-embedded graphene for CO oxidation in the presence of O_2 or N_2O. Although there has been no experimental evidence for the synthesis of Si-embedded graphene until now, Si-doping into other morphology of graphene, such as fullerenes [43–47] and nanotubes [48], has been reported in experiment. This suggests that it is quite possible to dope Si into graphene by adopting a similar method to Si-doped other carbon nanostructure. Similar to Si-doped nanotubes [48], Si-embedded graphene may also be synthesized using methoxytrimethylsilane as a precursor.

2 Computational models and methods

We carried out all-electron ab initio DFT calculations using double-numerical basis set with polarization function (the DNP basis set), implemented in the DMol^3 package [49, 50]. The spin-polarized Perdew–Burke–Ernzerhof (PBE) [51] functional within the generalized gradient approximation (GGA) was chosen for the DFT calculations. The used GGA/PBE method has also been successfully employed to study graphene systems in previous theoretical reports, including their interactions with various systems [39–41]. Full structural optimizations were performed without any symmetry constraints. Convergence in energy, force, and displacement was set as 10^{-5} Ha, 0.001 Ha/Å, and 0.005 Å, respectively. To ensure high-quality results, the real-space global orbital cutoff radius was chosen as high as 4.6 Å in the computations. The smearing of electronic occupations was set as 0.005 Ha.

A hexagonal graphene supercell (4×4 graphene unit cells) containing 32 atoms was introduced to model a system with one carbon atom substituted by one silicon atom. The modulus unit cell vector in the z direction was set to 15 Å, which is sufficiently large to avoid the interaction between the graphene and its periodic images. The Brillouin zone integration was performed with $3 \times 3 \times 1$ k points. To study the minimum-energy pathway (MEP) for CO oxidation, linear synchronous transit (LST/QST) and nudged elastic band (NEB) [52] tools in DMol^3 code were used, which have been well validated to search transition state (TS) and MEP [39–41]. The vibrational frequencies for each obtained structure along the MEP were calculated at the same level to ensure that every TS has a single-imaginary frequency and the stable local minimum has no imaginary frequency.

3 Results and discussion

3.1 The geometric structure and property of Si-embedded graphene

We started our study by investigating the geometric structure of Si-embedded graphene. As shown in Fig. 1a, the Si-atom is located on top of the single vacancy site, forming three bonds with the nearest C-atoms, in which the Si-atom preserves its sp^3 character. The bond length between Si-atom and each neighboring C-atom is 1.75 Å, which is much larger than that of the C–C bond of perfect graphene (1.42 Å). The 23 % increase in the bond length forces Si-atom to protrude from the graphene plane, also displacing the positions of the neighboring C-atoms out of the plane. Meanwhile, about 0.82 e is transferred from Si-atom to graphene sheet according to the Mulliken population analysis, and the whole system is nonmagnetic. The charge transfer can also be verified by the deformation electronic density of Si-embedded graphene (Fig. 1b), where the red and blue regions represent the areas of electron accumulation and loss, respectively. Here, the deformation electronic density was defined as the total electronic density excluding those of isolated atoms. One can see that different electron affinities of Si- and C-atom change the electron distribution of the whole system. Since the electrons are mainly located within the bonds rather than mainly located on the C-atoms, the whole graphene structure remains covalent in nature.

To gain deeper insights into the electronic structure of Si-embedded graphene, we further calculated its band structure and density of states (DOS). Compared to the band structure of the perfect graphene (Fig. 2a), the

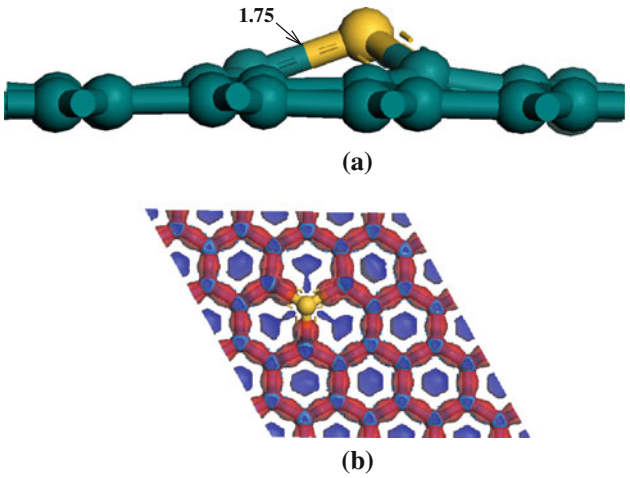

Fig. 1 **a** The geometric structures and **b** iso-surface (0.025 e/au) of the deformation electronic density of the Si-embedded graphene. The *yellow ball* represents the Si-atom. The *red* and *blue* regions show the electron accumulation and loss, respectively. The bond distances are in angstroms

minimum of the conduction band edge (CBM) of the graphene was found to be slightly shifted up, forming a small band gap of 0.05 eV (Fig. 2b). This is because Si-atom has four electrons in its valence shell, and it bounds with sp^3 hybridization. Meanwhile, Si-atom follows a pyramidal-like configuration, thus creating a localized state when bonded to a graphitic network, which would have little effects on the semi-metallic character of the graphene. Owing to the formation of three C–Si bonds and charge transfer from Si-atom to graphene, the Si-3s, Si-3p, and C-2p orbitals are partially filled, and strong hybridization between 3p states of Si-atom and 2p states of C-atoms of graphene can be observed above and below the E_F level (Fig. 2c). This indicates that the Si-atom uses its valence electrons to saturate the dangling bond states of the vacancy in graphene. Since the high DOS is localized around the Fermi level, the localized Si-3p states will play an important role in activating reactants to lower the reaction barrier. Additionally, the highest occupied electronic state (HOES) and the lowest unoccupied electronic state (LUES) at the gamma (Γ) point are displayed in Fig. 2d, e, respectively. The HOES is mainly contributed by the $3p_z$ atomic orbitals of the Si-atom. The LUES clearly shows three bonding between Si-atom and the nearest three C-atoms.

In light of the possible clustering problem of Si-atom embedded graphene, we also calculated the energy barrier (labeled as $E_{barrier}$) of the diffusion of Si-atom in graphene from the vacancy site to its neighboring bridge site (the Si-atom prefers the bridge site of the pristine graphene as shown in Figure S1 of the Supporting Information). The adsorption energy of Si-atom on the vacancy in graphene is −8.88 eV, which is much larger than that of pristine graphene (−0.46 eV). The diffusion energy barrier of Si-atom on defective graphene is about 6.82 eV, implying that Si clustering problem is absent and Si-embedded graphene is the energetically stable structure. To further confirm the stability of Si-embedded graphene, we performed vibrational frequency calculations. No imaginary frequencies are found, in which the lowest frequency is about 176.2 cm^{-1}, suggesting that this structure is dynamically stable. We also examined the thermal stability of Si-embedded graphene using the Born–Oppenheimer quantum molecular dynamics (MD) simulations with constant temperature of 300, 1,200, and 1,700 K. The Nosé–Hoover chain method was used for the temperature control. A default Nosé Q ratio of 2.0 (used to scale the fictitious mass) and a default Nosé chain length of 2 were selected. We found that after 5,000 time steps with the time step of 1 fs the system is distorted at 300 K, but can be re-optimized to previous static structure. More interestingly, it was found that the Si-embedded graphene can still be intact for 5 ps even at 1,700 K. The corresponding snapshot images of the equilibrium structures at 300, 1,200, and 1,700 K are listed in Figure S2. These results indicate that the Si-embedded graphene possesses high thermal stability.

3.2 Adsorptions of O_2, CO, N_2O, CO_2, N_2, and O on Si-embedded graphene

Before exploring the CO oxidation by O_2 or N_2O, we computed the adsorption of O_2, CO, N_2O, CO_2, N_2, and O on Si-embedded graphene, respectively. For each adsorbate, we considered various adsorption sites (including Si-atom and its nearest C-atom) and different adsorption patterns (including side-on and end-on). In Fig. 3, we listed the obtained most stable configurations for each adsorbate. The corresponding adsorption energies were shown in Table 1. For O_2 adsorption, the most stable adsorption configuration (Fig. 3a) is characterized by O_2 parallel to the graphene surface by forming two chemical bonds with Si-atom (side-on). Here, the singlet state is the ground state, so the original double bond of O_2 is transformed to a single bond. The adsorption energy of this configuration is −1.18 eV, which is 0.37 eV more favorable than that of the end-on configuration. Moreover, in this most stable configuration, the two formed Si–O bond lengths are 1.72 and 1.79 Å, respectively. There is about 0.71 e charge transfer from the embedded Si-atom to the $2\pi^*$ orbital of O_2, resulting in the elongation of the O–O bond of the adsorbed O_2 from 1.23 to 1.50 Å, a typical value of peroxo species [53]. In particular, as shown in Figure S3, the electrons mainly accumulate on O_2, where O_2-$2\pi^*$ orbital is half-filled, and the whole graphene structure is still covalent.

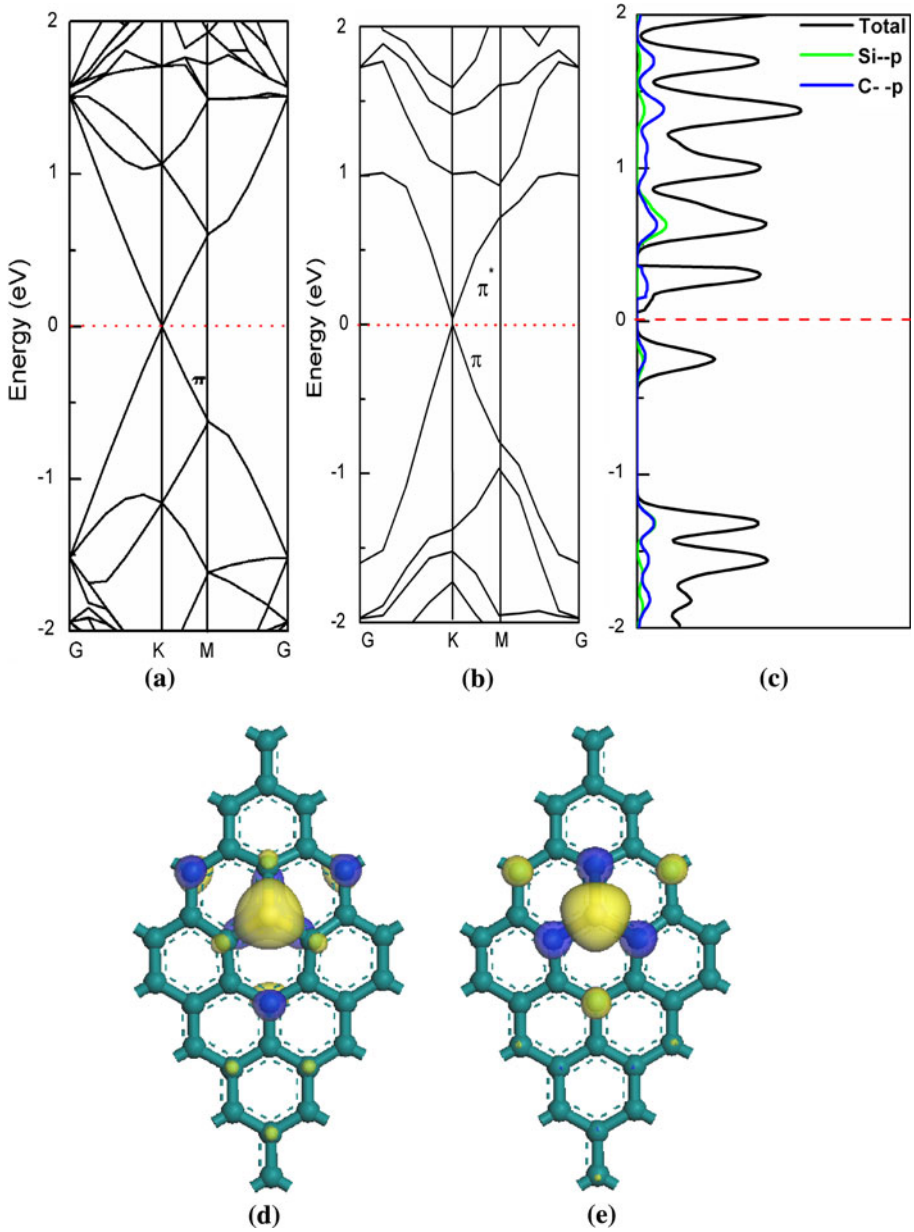

Fig. 2 Computed band structures of **a** pristine graphene and **b** Si-embedded graphene. **c** Projected density of states of Si-embedded graphene. **d** Iso-surface (the iso-value is 0.05 au) of the highest occupied electronic state, and **e** lowest unoccupied electronic state of Si-doped graphene at the Γ point

The end-on configuration (Fig. 3b) is the lowest energy form for CO adsorbed on Si-embedded graphene. This configuration has an adsorption energy of −0.17 eV, which is greatly less favorable than that of O_2 molecule (−1.18 eV). Thus, when CO/O_2 mixture is injected as the reaction gas, the Si-atom of Si-embedded graphene should be covered by O_2 molecule. Meanwhile, about 0.06 electron is transferred from Si-embedded graphene to the $2\pi^*$ orbital of CO, rendering the C–O length of CO elongate from 1.14 to 1.16 Å.

The presence of a preadsorbed O_2 molecule on the Si-atom can greatly enhance the interaction of CO molecule with Si-embedded graphene. We found that the CO molecule is energetically favorable to be attached to the nearest C-atom to the Si-atom in Si-embedded graphene, where a peroxy-type O1–O2–C–O complex is formed above Si-embedded graphene (Fig. 3c). The distance between CO and O_2/Si-embedded graphene is 1.59 Å, while one of the O-atoms of adsorbed O_2 escapes from the Si-atom and binds with CO molecule. The adsorption energy of CO + O_2 on Si-graphene is −2.56 eV. Compared to the sum of the adsorption energies of O_2 and CO [(−1.18) + (−0.17) = −1.35 eV], the net increase in the adsorption energy for the coadsorption of O_2 and CO amounts to 1.21 eV, indicating that a cooperative adsorption of CO and O_2 can occur the Si-embedded graphene. Meanwhile, there is about 0.32 *e* charge transfer from Si-embedded graphene to CO + O_2.

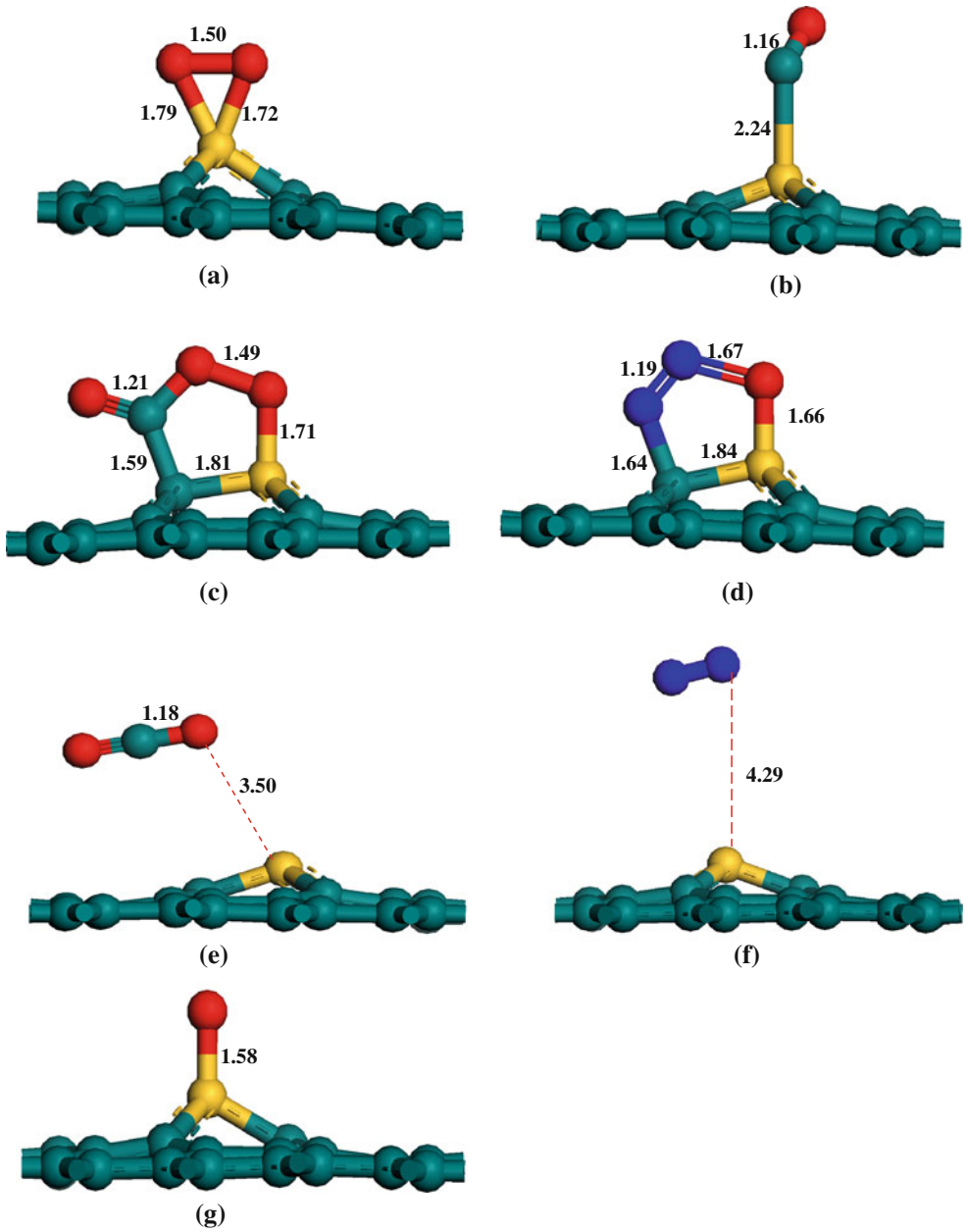

Fig. 3 The calculated most stable configurations structures of **a** O_2, **b** CO, **c** CO + O_2, **d** N_2O, **e** CO_2, **f** N_2, and **g** O on Si-embedded graphene. The *yellow*, *red*, and *blue balls* represent the Si, O, and N atom, respectively. The bond distances are in angstroms

For N_2O molecule, the most adsorption configuration is that the N- and O-atoms of N_2O bind with the Si–C bond via [3 + 2] cycloaddition, forming a five-membered ring (Fig. 3d). The calculated adsorption energy is −0.37 eV, which is larger than that of CO (−0.17 eV). There is 0.22 *e* to be transferred from Si-embedded graphene to N_2O-$3\pi^*$ orbital, leading to the great decrease in the N–N–O angle of N_2O from 180° to 115°. The most stable adsorption site of CO_2 (Fig. 3e) or N_2 (Fig. 3f) locates on Si-atom of Si-embedded graphene (end-on configuration) via researching various possible adsorption sites. The small adsorption energy (−0.06 eV for CO_2 and −0.06 eV for N_2) indicates that the attachment of CO_2 or N_2 to Si-embedded graphene is very weak, which is further testified by the small charge transfer and large distance between adsorbate and graphene (Table 1). Hence, it is easy for CO_2 or N_2 to desorb from the surface of Si-embedded graphene. In addition, the atomic O can strongly bind to the embedded Si-atom with $E_{ads}(O) = -6.09$ eV as shown in Fig. 3g.

Table 1 Adsorption energy (E_{ads})[a] of various adsorbates on the Si-embedded graphene, the charge transfer (Q)[b], and the shortest distance (d) between the adsorbate and Si-embedded

Adsorbate	E_{ads} (eV)	Q (e)	d (Å)
O_2	−1.18	−0.71	1.72
CO	−0.17	−0.06	2.24
CO + O_2	−2.56	−0.32	1.59 (CO)/1.71 (O_2)
N_2O	−0.22	−0.49	1.66
CO_2	−0.06	0.01	3.50
N_2	−0.06	0.00	4.29
O	−6.09	−0.64	1.58

[a] Adsorption energy is defined as $E_{ads} = E_{total}$ [Si-embedded graphene + adsorbate] − E_{total} [Si-embedded graphene] − E_{total} [adsorbate], where E_{total} is the total energy of the system per supercell

[b] The charge transfer is calculated through Mulliken population analysis

3.3 Mechanisms for CO oxidation by O_2 or N_2O on Si-embedded graphene

We investigated both the Eley–Rideal (ER) and Langmuir–Hinshelwood (LH) mechanisms of CO oxidation on Si-embedded graphene. For the ER mechanism, the gas-phase CO molecule approaches the already-activated O_2 or N_2O. The LH mechanism involves the coadsorption of CO and O_2 (or N_2O) molecules before reaction. Li et al. [40] proposed theoretically that Fe atom embedded with graphene are active and stable catalysts for CO oxidation via the more favorable ER mechanism with a two-step route ($E_{barrier} = 0.58$ eV), while LH reaction is shown to be a starting point for CO oxidation on Au- and Cu-embedded graphene with the activation barriers of 0.31 and 0.25 eV, respectively [39, 41]. In terms of the above evidences, the following questions arise: (1) can CO molecule also be oxidized on ***metal-free*** Si-embedded graphene? (2) If can, which mechanism (ER and LH) is more favorable for CO oxidation by O_2 or N_2O? And, what is the barrier energy of CO oxidation by O_2 or N_2O on Si-embedded graphene?

To resolve the above questions, we computed the MEP for CO oxidation by O_2 or N_2O on Si-embedded using NEB method, in which both ER and LH mechanisms are comparably studied. For CO oxidation by O_2 via ER mechanism, it was found that the energy barrier is as high as 0.99 eV (see Figure S4), much larger than that of LH mechanism (Fig. 4). Thus, for CO oxidation by O_2 on Si-embedded graphene, LH mechanism is more favorable than ER one. On the basis of the above reasons, we considered the LH reaction, that is, CO + O_2 → OOCO → CO_2 + O is used as a starting point, followed by the ER reaction CO + O → CO_2. To search for the MEP for this reaction, we selected an initial state (IS) configuration as shown in Fig. 5, that is, CO is physisorbed adsorbed on the Si-embedded graphene, in which O_2 is located at the Si-atom. The final state (FS) is that a CO_2 molecule physisorbed on Si-embedded graphene with a chemisorbed atomic O nearby. To achieve sufficient accuracy, 20 image structures were inserted between the IS and FS, and the corresponding MEP profile is summarized in Fig. 4. The energetics is schematically plotted with respect to the reference energy, which is the sum of the energies of the Si-embedded graphene and individual CO and O_2 molecules, assuming that CO and O_2 are far apart. The local configurations of the adsorbates on the Si-embedded graphene at various states along the MEP are displayed in Fig. 5. The CO + O_2 reaction pathway is characterized as a proxy-type O–O–C–O intermediate state (labeled as MS).

It can be seen from Fig. 5 that the CO molecule starts to approach C-atom neighboring to Si-atom at the reaction to reach the first transition state (TS1), resulting in the physisorption of CO on Si-embedded graphene with an energy barrier of 0.48 eV along the reaction pathway. Meanwhile, the distance between CO and graphene is decreased from 3.63 (IS) to 3.14 Å (TS1). Passing over TS1, a peroxo-type O–O–C–O complex (MS) is formed, which is 1.70 eV lower in energy than TS1. Furthermore, the O–O bond length of MS is continually elongated from 1.49 to 1.89 Å, and the system reaches the second transition state (TS2). Passing over TS2 with a relatively low barrier of 0.21 eV, a CO_2 molecule is formed, leaving an atomic O adsorbed on the Si-atom. It is easy for the formed CO_2 to escape from the surface of Si-embedded graphene at room temperature due to its weak interaction with this graphene.

On the other hand, when N_2O molecule is used to oxidize CO into CO_2, Si-embedded graphene will be dominantly

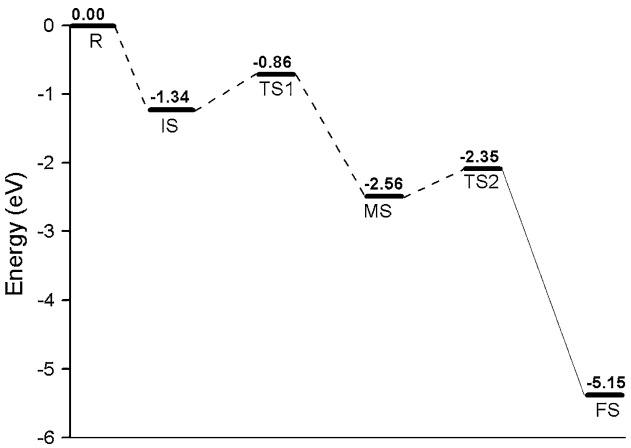

Fig. 4 Schematic energy profile corresponding to local configurations shown in Fig. 5 along the minimum-energy pathway via the CO + O_2 → OOCO → CO_2 + O route. All energies are given with respect to the reference energy, that is, the sum of energies of Si-embedded graphene and individual CO and O_2 molecules

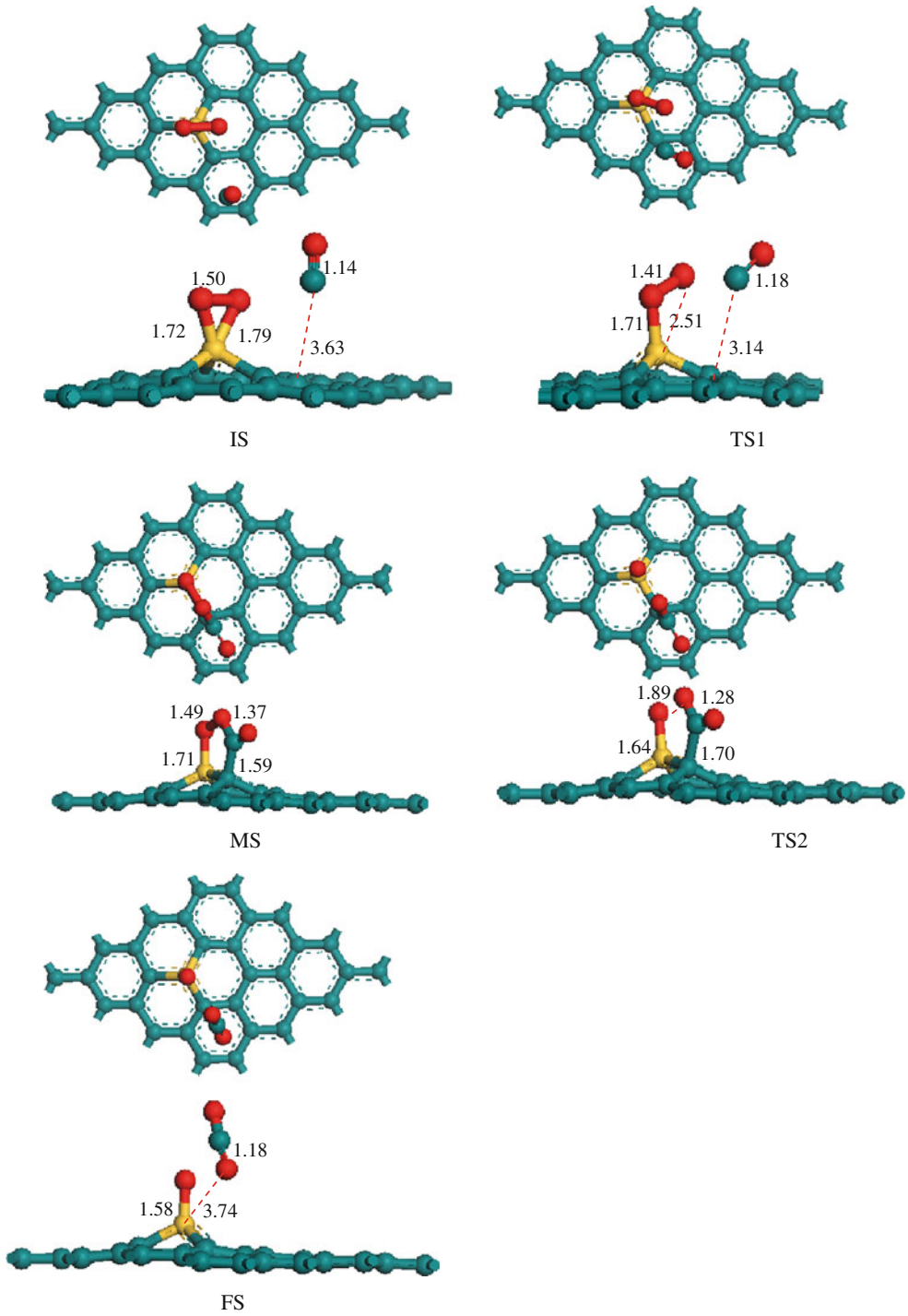

Fig. 5 Local configurations of the adsorbates on the Si-embedded graphene at various intermediate states, including the initial state (IS), transition state (TS), metastable state (MS), and final state (FS) along the minimum-energy pathway via the $CO + O_2 \rightarrow OOCO \rightarrow CO_2 + O$ route. Both side (*upper panel*) and *top* (*lower panel*) views are displayed. The *yellow* and *red balls* represent the Si- and O-atom, respectively. The bond distances are in angstroms

covered by N_2O molecules if CO/N_2O mixture is injected as the reaction gas because Si-embedded graphene has slightly stronger interactions with N_2O ($E_{ads} = -0.37$ eV) than that of CO ($E_{ads} = -0.17$ eV) from the energetic point of view. For the adsorbed N_2O, we found that the N–O and N–C bonds can be continually elongated to reach a TS as shown in Fig. 6. The N–O and N–C bond lengths in this TS are increased from 1.67 and 1.64 to 1.70 and 1.67 Å, respectively. The energy barrier of this process is estimated to be 0.02 eV. Crossing the TS, a N_2 molecule is formed, leaving

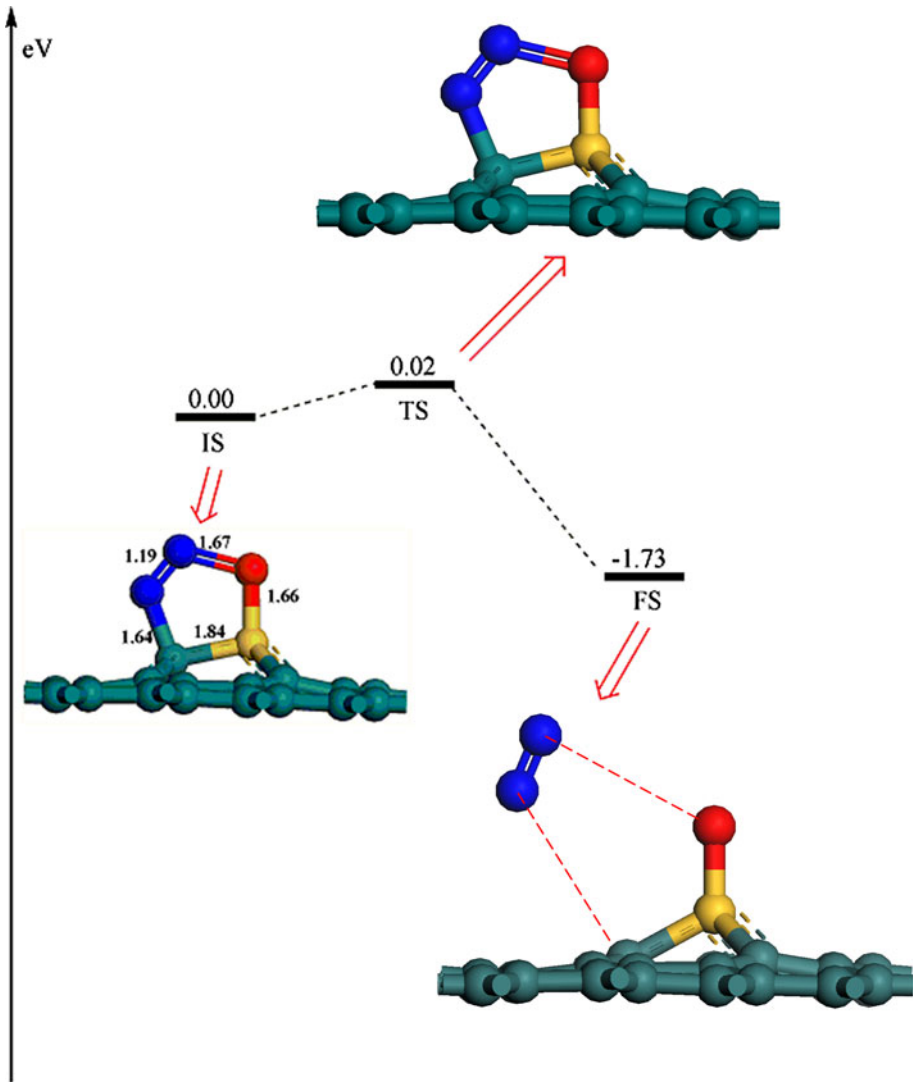

Fig. 6 The reaction path along the minimum-energy pathway via $N_2O \rightarrow N_2 + O$ route and the corresponding local configurations of the adsorbates on Si-embedded graphene

an atomic O adsorbed on Si-atom. Due to the weak interaction between N_2 and the Si-embedded graphene ($E_{ads} = -0.06$ eV), the N_2 molecule can be easily desorbed at room temperature. The energy released in this step is -1.73 eV. In light of the small barrier (0.02 eV) and large exothermicity (1.73 eV), it is expected that the dissociation of N_2O can be achieved quite easily. That is, when N_2O is used as a reactant for CO oxidation, it first dissociates into N_2 molecule and O-atom. Thus, the ER mechanism is possible as a starting point, which is completely different from the case of CO oxidation by O_2.

Since an atomic O is left on Si-embedded graphene in the process of CO oxidation by O_2 or N_2O, it is very necessary to explore whether this atomic O can be further reduced by subsequent CO molecule via ER mechanism. A configuration of physisorbed CO on the C-atom near to Si-atom is chosen as the IS (Fig. 7a). The FS is set to the configuration of CO_2 adsorbed on the Si-embedded graphene (Fig. 3d). The results indicate that the C-atom of CO first approaches the adsorbed O-atom to reach a TS. The distance between CO and the O-atom is shortened from 2.89 of IS to 1.97 Å of TS in this endothermic process. It is clearly seen from Fig. 8 that a very small barrier (0.14 eV), about a third of the barrier of the LH mechanism for the $CO + O_2$ reaction (0.48 eV), separates the IS and the MS along the MEP. Passing over the MS with an energy barrier of 0.57 eV, a CO_2 molecule is formed, leading to the recovery of Si-embedded graphene. It should be pointed out that, in the catalysis theory, the overall barrier is important rather than a particular barrier. Usually, if one of the intermediate reactions is endothermic, the overall barrier can be higher than all the particular ones. Otherwise, the overall barrier should be equal to the highest particular one [41]. As shown in Fig. 8, both the intermediate and final reactions of $CO + O \rightarrow CO_2$ are exothermic with barriers of 0.14 and 0.57 eV. Thus, the overall barrier of $CO + O \rightarrow CO_2$ should be equal to the latter one, namely 0.57 eV, which is the rate-limiting

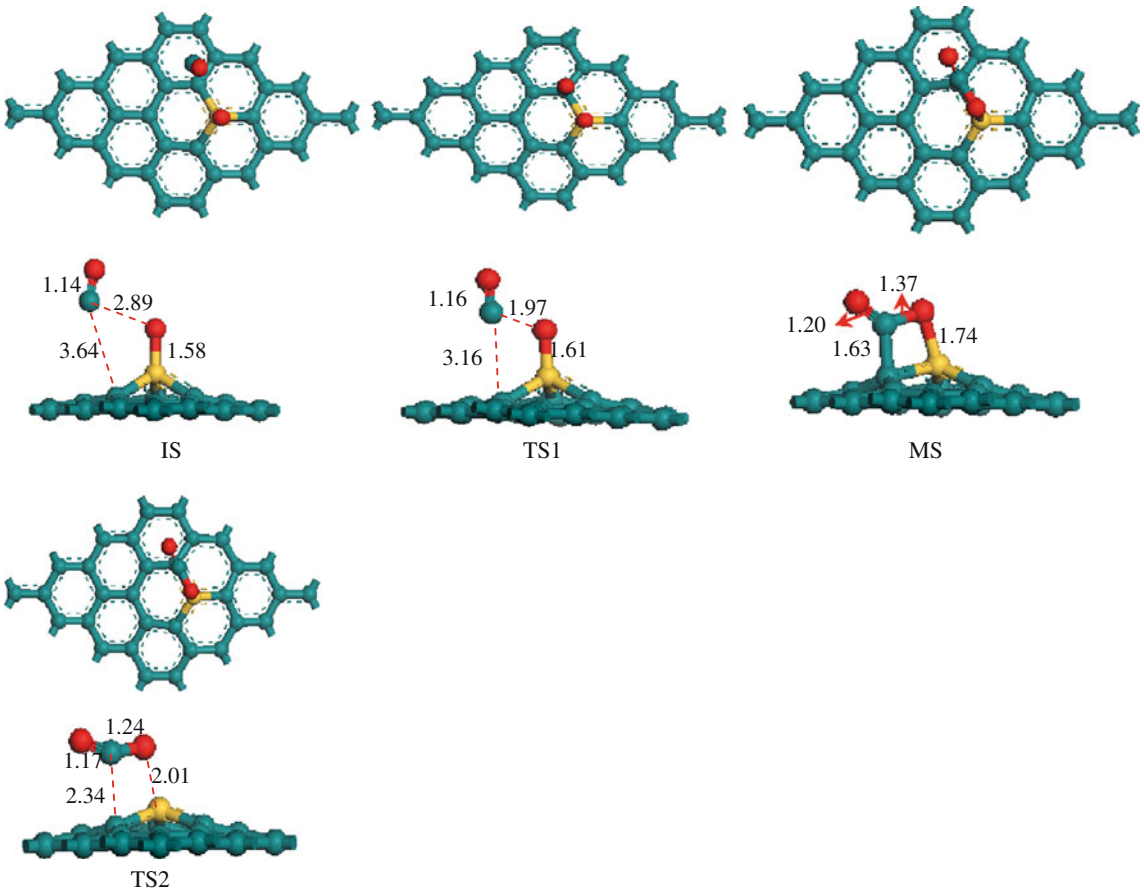

Fig. 7 Local configurations of the adsorbates on the Si-embedded graphene at various intermediate states, including the initial state (IS), transition state (TS), metastable state (MS), and final state (FS) along the minimum-energy pathway via the CO + O → CO_2 route. Both side (*upper panel*) and *top* (*lower panel*) views are displayed. The *yellow* and *red balls* represent the Si- and O-atom, respectively. The bond distances are in angstroms

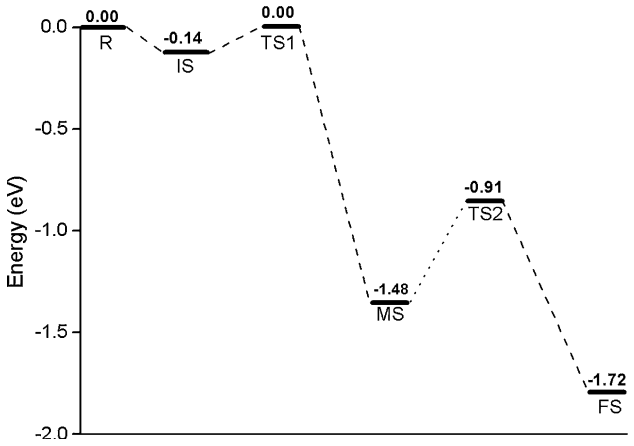

Fig. 8 Schematic energy profile corresponding to local configurations (Fig. 7) along the minimum-energy pathway via the CO + O_2 → CO_2 route

step and corresponds to the desorption of CO_2 from Si-embedded graphene.

On the basis of the above discussions, we expected that the CO oxidization by O_2 and N_2O on the Si-embedded graphene may be characterized as a two-step process: (1) for CO oxidization by O_2, the LH reaction initiates the CO oxidation ($E_{barrier}$ = 0.48 eV), while the N_2O is first efficiently activated by Si doptant via ER reaction in the case of CO oxidation by N_2O ($E_{barrier}$ = 0.02 eV); (2) in the second step of CO oxidation by O_2 and N_2O, the reaction of CO + O → CO_2 occurs via ER mechanism (0.57 eV). The above results indicate that the catalytic activity toward CO oxidation of Si-embedded graphene can be comparable to that of Fe-, Au-, or Cu-graphene [39–41], in which the energy barriers for CO oxidation are 0.58, 0.31, and 0.25 eV, respectively.

Notably, it is known that van-der-Waals (vdW) correction to account for dispersion interactions is very important for graphene-based systems due to the low chemical activity of pristine graphene. Thus, using Grimme scheme [54], we take the first step of CO oxidation by O_2 on Si-embedded graphene as an example to re-calculate the adsorption energies, reaction energetics, and inter-atomic distances in adsorption complexes and transition states with a vdW correction. The results indicate that the

adsorption energies of O_2, CO, CO_2, and CO + O_2 on Si-embedded graphene are −1.37, −0.33, −0.11, and −2.93 eV, respectively, which are slightly larger than those of using pure PBE functional (−1.18, −0.17, −0.06, and −2.56 eV for O_2, CO, CO_2, and CO + O_2, respectively). Moreover, it is found that the distances between adsorbates and Si-embedded are independent on the used methods. As shown in Figure S5, the barrier of this step with a vdW correction is calculated to be 0.50 eV, which is slightly larger than the case using pure PBE functional (0.48 eV). Overall, the adsorption energies, reaction energetics, and energy barrier are slightly increased due to the vdW correction, while the geometric structures of adsorption complexes and transition states are unchanged.

4 Conclusion

Using DFT, we have explored the possibility of Si-embedded graphene as a potential ***metal-free*** catalyst for CO oxidation by O_2 or N_2O. The results indicated that the Si-embedded graphene exhibits high catalytic activity for CO oxidation. The catalytic process is likely to proceed with the LH reaction at the starting point for CO oxidation by O_2 with a low activation barrier of 0.48 eV. When N_2O is used to oxide CO, it is firstly reduced into N_2 + O_{ads} with a much smaller energy barrier (0.02 eV). Then, the left O-atom can be pulled away by the subsequent CO from the Si-embedded graphene via the ER mechanism. In this process, a total energy barrier of 0.57 eV has to be overcome. The present work suggests that Si-embedded graphene is an efficient and ***metal-free*** catalyst for CO oxidation, and future experimental studies are greatly desired to probe such interesting processes.

Acknowledgments We gratefully acknowledge the support of this research by the Key Program Projects of the National Natural Science Foundation of China (No. 21031001), the National Natural Science Foundation of China (No. 20971040), the Cultivation Fund of the Key Scientific and Technical Innovation Project, Ministry of Education of China (No. 708029), the Key Program Projects of the Province Natural Science Foundation of Heilongjiang Province (No. ZJG0602-01), the National Basic Research Priority Program (No. 2007CB914104), the China Postdoctoral Science Foundation (20110491119), Heilongjiang Postdoctoral Science Foundation (LBH-Z10049), and Committee of Education of Heilongjiang Province (11541095). The authors would like to show great gratitude to the reviewers for raising invaluable comments and suggestions.

References

1. Freund H-J, Meijer G, Scheffler M, Schlögl R, Wolf M (2011) Angew Chem Int Ed 50:2 and therein references (recent review)
2. Nakai L, Kondoh H, Shimada T, Resta A, Andersen JN, Ohta T (2006) J Chem Phys 124:224712
3. Eichler A (2002) Surf Sci 498:314
4. Zhang CJ, Hu P (2001) J Am Chem Soc 123:1166
5. Salo P, Honkala K, Alatalo M, Laasonen K (2002) Surf Sci 516:247
6. Chen MS, Cai Y, Yan Z, Gath KK, Axnanda S, Goodman DW (2007) Surf Sci 601:5326
7. Oh S-H, Hoflund GB (2007) J Catal 245:35
8. Liu W, Zhu YF, Lian JS, Jiang Q (2006) J Phys Chem C 111:1005
9. Ackermann MD, Pedersen TM, Hendriksen BLM, Robach O, Bobaru SC, Popa I, Quiros C, Kim H, Hammer B, Ferrer S, Frenken JWM (2005) Phys Rev Lett 95:255505
10. Nakai I, Kondoh H, Amemiya K, Nagasaka M, Nambu A, Shimada T, Ohta T (2004) J Chem Phys 121:5035
11. Alavi A, Hu P, Deutsch T, Silvestrelli PL, Hutter J (1998) Phys Rev Lett 80:3650
12. Eichler A, Hafner J (1999) Surf Sci 435:58
13. Bleakley K, Hu P (1999) J Am Chem Soc 121:7644
14. Krenn G, Bako I, Schennach R (2006) J Chem Phys 124:144703
15. Sljivancanin Z, Hammer B (2010) Phys Rev B 81:121413
16. Liu DJ (2007) J Phys Chem C 111:14698
17. Stampfl C, Scheffler M (1999) Surf Sci 433:119
18. Kimble ML, Castleman AW, Mitrić R, Bürgel C, Bonačić-Koutecký V (2004) J Am Chem Soc 126:2526
19. Socaciu LD, Hagen J, Bernhardt TM, Wöste L, Heiz U, Häkkinen H, Landman U (2003) J Am Chem Soc 125:10437
20. Lopez N, Nørskov JK (2002) J Am Chem Soc 124:11262
21. Liu ZP, Hu P, Alavi A (2002) J Am Chem Soc 124:14770
22. Kandoi S, Gokhale AA, Grabow LC, Dumesic JA, Mavrikakis M (2004) Catal Lett 93:93
23. Geim AK (2009) Science 324:1530
24. Rao CNR, Sood AK, Subrahmanyam KS, Govindaraj A (2009) Angew Chem Int Ed 48:7752
25. Rao CNR, Biswas K, Subrahmanyam KS, Govindaraj A (2009) J Mater Chem 19:2457
26. Neto AHC, Guinea F, Peres NMR, Novoselov KS, Geim AK (2009) Rev Mod Phys 81:109
27. Taghioskoui M (2009) Mater Today 12:34
28. Zhu Y, Murali S, Cai W, Li X, Suk JW, Potts JR, Ruoff RS (2010) Adv Mater 22:3906
29. Schedin F, Geim AK, Moeozov SV, Hill EW, Blake P, Katsnelson MI, Novoselov KS (2007) Nat Mater 6:652
30. Barbolina II, Novoselov KS, Morozov SV, Dubonos SV, Missous M, Volkov AO, Christian DA, Grigorieva IV, Geim AK (2006) Appl Phys Lett 88:013901
31. Allen MJ, Tung VC, Kaner RB (2010) Chem Rev 110:132
32. Loh KP, Bao Q, Ang PK, Yang J (2010) J Mater Chem 20:2277
33. Terronesa M, Botello-Méndez AR, Campos-Delgado J, López-Urías F, Vega-Cantú YI, Rodríguez-Macías FJ, Elías AL, Muñoz-Sandoval E, Cano-Márquez AG, Charlier J-C, Terrones H (2010) Nanotoday 5:351
34. Abergel DSL, Apalkov V, Berashevich J, Ziegler K, Chakraborty T (2010) Adv Phys 59:261
35. Choi W, Lahiri L, Seelaboyina R, Kang YS (2010) Crit Rev Solid State Mater Sci 35:52
36. Yang J, Tian CG, Wang L, Fu HG (2011) J Mater Chem 21:3384
37. Rao CV, Reddy ALM, Ishikawa Y, Ajayan PM (2011) Carbon 49:931
38. Yoo E, Okata T, Akita T, Kohyama M, Nakamura J, Honma I (2009) Nano Lett 9:2255
39. Lu Y-Y, Zhou M, Zhang C, Feng Y-P (2009) J Phys Chem C 113:20156
40. Li Y, Zhou Z, Yu G, Chen W, Chen Z (2010) J Phys Chem C 114:6250
41. Song EH, Wen Z, Jiang Q (2011) J Phys Chem C 115:3678

42. Su DS, Zhang J, Frank B, Thomas A, Wang X, Paraknowitsch J, Schlögl R (2010) ChemSusChem 3:169
43. Fye JL, Jarrold MF (1997) J Phys Chem A 101:1836
44. Kimura T, Sugai T, Shinohara H (1996) Chem Phys Lett 256:269
45. Ray C, Pellarin M, Lermé JL, Vialle JL, Broyer M, Blasé X, Mélinon P, Kéghélian P, Perez A (1998) Phys Rev Lett 80:5365
46. Pellarin M, Ray C, Lermé JL, Vialle JL, Broyer M, Blasé X, Kéghélian P, Mélinon P, Perez A (1999) J Chem Phys 110:6927
47. Bulina NV, Lopatin VA, Vnukova NG, Osipova IV, Churilov GN, Krätschmer W (2007) Fuller Nanotub Carbon Nanosturcut 15:395
48. Campos-Delgado J, Maciel IO, Cullen DA, Smith DJ, Jorio A, Pimenta MA, Terrones H, Terrones M (2010) ACS Nano 4:1696
49. Delley B (1990) J Chem Phys 92:508
50. Delley B (2000) J Chem Phys 113:7756
51. Perdew JP, Burke K, Ernzerhof M (1996) Phys Rev Lett 77:3865
52. Henkelman G, Jonsson H (2000) J Chem Phys 113:9978
53. Gutsev GL, Rao BK, Jena P (2000) J Phys Chem A 104:11961
54. Grimme S (2006) J Comput Chem 27:1787